Jamming of hard rods I: From Onsager to Edwards

Maximilien Danisch[1,2], Adrian Baule[2], and Hernan A. Makse[2]
[1] *Physics Department, Ecole Normale Supérieure de Cachan, 61 Avenue du President Wilson, 94235 Cachan, France*
[2] *Levich Institute and Physics Department, City College of New York, New York, NY 10031, US*

In a 1949 iconic paper, Onsager demonstrated the existence of a first-order isotropic-to-nematic transition as the density of an equilibrium suspension of infinitely thin hard rods is increased. When the particles in the suspension settle under gravity a new jammed phase emerges. Jammed states show reversible behavior when systematically shaken, and therefore, can be treated by statistical mechanics as proposed by Edwards. We develop a route to study the phases of jammed packings of rodlike particles under the umbrella of Edwards ensemble by extending the framework of Song *et al.*, Nature (2008) from hard spheres to hard spherocylinders. In this paper, we start by calculating the Voronoi diagram of a set of spherocylinders and present an algorithm for its evaluation. We then discuss the next steps to develop the Edwards ensemble in search of novel phases of jammed matter of hard rodlike particles.

I. INTRODUCTION.

Packings of rods in three dimensions have been extensively studied due to their rich theoretical [1] and industrial aspects with applications to lyotropic liquid crystals, bio-packings like DNA, powders and construction materials [2]. This rich behavior is related to the number of degrees of freedom, which gives rise to interesting liquid crystal phases beyond the usual crystal-liquid-gas phases. However, the existence of intrinsic correlations seems to prohibit any theoretical study so far attempted, except for infinitely thin hard rods in thermal equilibrium, where these correlations vanish as shown by Onsager's virial theory [3]: Onsager's second order truncation of the free energy becomes exact in the limit of infinitely thin particles [1].

When a suspension of rods settles by gravity, a jammed phase develops where each particle is at mechanical equilibrium and thermal agitation does not play a role. The present paper is the starting point of a series that will investigate the jammed phases of packings of rods from a statistical mechanical point of view using Edwards' ensemble theory for jammed granular matter [4]. The applicability of the theory to the study of same-size ball packings in two [5], three [6–8], and infinite dimensions [9] and for polydisperse ball packings [10] motivates the present work. As in Onsager's equilibrium theory, rodlike jammed particles of different orientations can be treated as belonging to different species. Thus, the problem of non-spherical monodisperse particles can be mapped to the problem of polydisperse spheres and the framework developed in [10] for jamming of different size balls can be readily applied to the jamming of hard rods.

This paper is mainly technical and presents an algorithm for the calculation of the Voronoi diagram of a set of spherocylinders. The Voronoi volume of a single particle in Edwards' statistical mechanics (also called the *volume function* [4]) is the analogue of the energy associated to a particle in the classical Boltzmann statistical mechanics. We study spherocylinders (a cylinder of length L and diameter $D = 2a$ capped with two semispheres of radius a at both ends) as a model of hard rods since their Voronoi diagram is the same as the one of line segments. Spherocylinders constitute therefore a special case of non-spherical particles which are easier to treat than, for instance, ellipsoids of revolution. However, the general concepts are expected to apply to these more complicated shapes as well. The limiting aspect ratio $L/D \to \infty$ is discussed as a generalization of Onsager's equilibrium results as well as the spherical limit, $L/D = 0$, as a generalization of the equilibrium phases of hard spheres.

The following results are relevant for the present study:

(i) Onsager's theory for equilibrium thin rods [1, 3], $L/D \to \infty$, predicts a first order transition between an isotropic phase stable below the freezing point at the volume fraction $\phi^{\mathrm{rod-eq}}_{\mathrm{freez}} L/D \approx 3.29$, and a nematic phase stable above the melting point $\phi^{\mathrm{rod-eq}}_{\mathrm{melt}} L/D \approx 4.19$.

(ii) Onsager's transition is analogous to the freezing transition of equilibrium hard spheres ($L/D = 0$) [11, 12] between an isotropic phase stable below $\phi^{\mathrm{sph-eq}}_{\mathrm{freez}} = 0.494 \pm 0.002$ and a crystalline phase stable above $\phi^{\mathrm{sph-eq}}_{\mathrm{melt}} = 0.545 \pm 0.002$.

(iii) Philipse *et al.* experimentally studied isotropic jammed phases of thin rods [13] and showed that the volume fraction of the random close packing (RCP) as a function of aspect ratio can be fitted as $\phi^{\mathrm{rod-jam}}_{\mathrm{rcp}} L/D \sim c$. This formula is valid for $L/D \gg 1$ and has been related to excluded volume arguments from Onsager [13] showing that $c = 5.4 \pm 0.2$ is half the isostatic coordination number of rods, $Z^{\mathrm{rod}}_{\mathrm{iso}} = 10$. When $L/D \to 0$ new physics beyond the Onsager limit appears as the isostatic limit of spherical particles $Z^{\mathrm{sph}}_{\mathrm{iso}} = 6$ is approached continuously from $Z^{\mathrm{rod}}_{\mathrm{iso}}$ [14].

(iv) Jin *et al.* [15] found numerically that jammed hard spheres undergo a first-order phase transition analogous to the equilibrium one. This scenario has been proposed by Radin *et al.* [16, 17]. The jammed isotropic phase is stable from random loose packing, RLP, $\phi^{\mathrm{sph-jam}}_{\mathrm{rlp}} \approx 0.536$, to RCP, $\phi^{\mathrm{sph-jam}}_{\mathrm{rcp}} \equiv \phi^{\mathrm{sph-jam}}_{\mathrm{freez}} \approx 0.634$ [6]. The

crystal phase is stable from the melting point $\phi_{\rm melt}^{\rm sph-jam} \approx 0.68$ to FCC, $\phi_{\rm fcc}^{\rm sph-jam} = \pi/\sqrt{18} \approx 0.740$. Between melting and freezing a glass-crystal mixture coexists.

(v) The application of the Edwards ensemble to jammed elongated particles has been treated by Mounfield and Edwards [18]. This approach uses a phenomenological mean-field volume function to describe the microscopic interactions between rods. The phase behavior predicted by Mounfield and Edwards is rather simple with no evidence of a discontinuous change in the symmetry of the system, suggesting no phase transition in contrast to Onsager's model. We notice that Edwards' model, being phenomenological, does not explicitly take into account the steric interaction between rods.

Here we calculate a volume function based on the Voronoi volume which accounts for excluded volume effects and orientational interactions, crucial to determine the phase behavior of the system. The purpose of the present work is to investigate the phases of jammed rods for all aspect ratios.

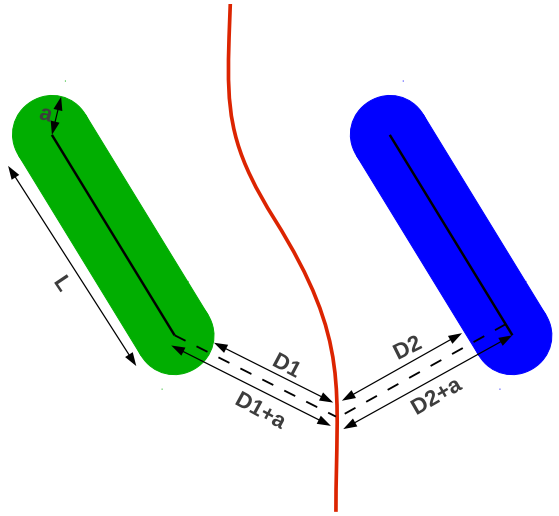

FIG. 1: Voronoi diagram equivalence between two spherocylinders and two line segments defining the spherocylinders. The Voronoi boundary is equivalent to that of two rods of vanishing width and length L, i.e., solving for the point where $D_1 = D_2$ is the same as solving $D_1 + a = D_2 + a$.

II. EQUIVALENCE BETWEEN THE VORONOI DIAGRAM OF SPHEROCYLINDERS AND SEGMENTS

For the study of jammed packings, Edwards' ensemble theory uses the volume as a conserved quantity instead of the energy as in the classical Boltzmann statistical mechanics. The volume associated to each particle is the Voronoi volume [6] defined as all the points of the space that are nearer to the particle than to any other one. The Voronoi boundary between two particles is then the hypersurface that contains all the points that are equidistant to both objects (Fig. 1).

In geometry, the calculation of the Voronoi diagram of a set of ellipsoids is an old and complicated problem. The calculation of the Voronoi diagram of spherocylinders is simpler than the one for ellipsoids thanks to the following property: the Voronoi diagram of a set of spherocylinders of length L and radius a is equivalent to the one of segments of length L, see Fig. 1. This equivalence is analogous to the case of equal size spheres. The Voronoi diagram of spheres can be calculated by considering only the set of sphere centers. Such equivalence disappears for instance, when the system consists of spheres of different size.

The radius a of the spherocylinders thus does not appear explicitly in the calculation of the Voronoi boundary as outlined in the next sections. However, the radius enters naturally as a limiting condition for the possible configurations of the spherocylinders: for given orientations of the spherocylinders the radius determines a minimal separation such that the volumes are not overlapping.

Furthermore, since the Voronoi diagram of a set of objects can be deduced from the one between every pair of objects, the problem is reduced to the calculation of the Voronoi boundary between two segments. This Voronoi boundary is composed of nine analytical surfaces that have to be evaluated and properly cut to define the continuous and differentiable Voronoi boundary. These surfaces arise as the Voronoi boundary due to the following interactions which must be treated separately: a *point-point* interaction between any two ends of the segments (four interactions in total), a *line-point* interaction between one segment and the end of the other segment (four interactions), and a *line-line* interaction between the two segments (one interaction). The principle of the algorithm is the calculation of these nine surfaces and determine where to cut them to form a continuous and differentiable Voronoi boundary.

III. PARAMETRIZATION OF THE PROBLEM

We use the parameters displayed in Fig. 2.

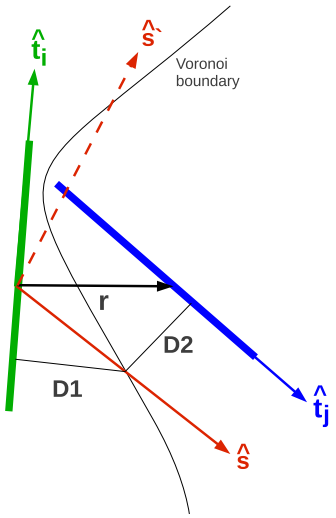

FIG. 2: Parametrization of the problem.

Let us set the origin of the coordinate system at the center of rod i, the vector $\vec{r}$ points to the center of the rod j. We are interested in the calculation of the Voronoi boundary along a generic direction $\vec{s} = s\hat{s}$ parameterized by s. A point on rod i is denoted by the vector $\vec{t}_i$ and a point on rod j by $\vec{t}_j$, where $\vec{t}_j$ originates at the center of rod j, i.e., $\hat{t}_i$ and $\hat{t}_j$ denote the directions of rods i and j, respectively, such that: $\vec{t}_i = t_i\hat{t}_i$, with $t_i \in [-L/2; L/2]$, and analogously for $\vec{t}_j$.

In the following we use the convention that a vector $\vec{a}$ can be decomposed as $\vec{a} = a\hat{a}$, where a denotes the absolute value and $\hat{a}$ the unit direction. The product of two vectors $\vec{a}\vec{b}$ denotes the scalar product $\vec{a}\cdot\vec{b} = \sum_k a_k b_k$, where the sum is over all components.

The Voronoi boundary is obtained from two conditions:

(i) The point $\vec{s}$ has the minimal distance to both rod i and rod j in the direction $\hat{s}$, and

(ii) both distances are the same.

The square of the distance D_i between $\vec{t}_i$ and $\vec{s}$ and D_j between $\vec{t}_j$ and $\vec{s}$ are

$$D_i^2 = (\vec{t}_i - \vec{s})^2, \tag{1a}$$
$$D_j^2 = (\vec{r} + \vec{t}_j - \vec{s})^2. \tag{1b}$$

Condition *(i)* then requires:

$$\frac{\partial D_i^2}{\partial t_i} = 0, \tag{2a}$$
$$\frac{\partial D_j^2}{\partial t_j} = 0. \tag{2b}$$

This leads to the minimal values along $\vec{t}_i$ and $\vec{t}_j$, respectively:

$$t_i^{\min} = \vec{s}\hat{t}_i = s(\hat{s}\hat{t}_i), \tag{3a}$$
$$t_j^{\min} = (\vec{s} - \vec{r})\hat{t}_j = s(\hat{s}\hat{t}_j) - r(\hat{r}\hat{t}_j). \tag{3b}$$

Condition *(ii)* requires:

$$D_i^{\min} = D_j^{\min}, \tag{4}$$

which leads to:

$$(t_i^{\min}\hat{t}_i - \vec{s})^2 = (t_j^{\min}\hat{t}_j + \vec{r} - \vec{s})^2. \tag{5}$$

The solution of Eqs. (2) and (4) depends on the type of interactions between the rods as discussed above. We distinguish the four generic cases:

1. *Line-line* interaction: $t_i^{\min} \in [-L/2, L/2]$ and $t_j^{\min} \in [-L/2, L/2]$ (one case).
2. *Line-point* interaction between the segment i and an end-point of j: $t_i^{\min} \in [-L/2, L/2]$ and $t_j = \pm L/2$ (2 cases).
3. *Point-line* interaction between the segment j and an end-point of i: $t_j^{\min} \in [-L/2, L/2]$ and $t_i = \pm L/2$ (2 cases).
4. *Point-point* interaction between the end points of i and j: $t_i = \pm L/2$ and $t_j = \pm L/2$ (4 cases).

By solving Eq. (5) for s, under the conditions that s has to be real and positive, one obtains the Voronoi boundary at $\vec{s} = s\hat{s}$. The solution of Eq. (5) depends on the type of interactions between the rods as discussed above. We distinguish the four generic cases:

1. *Line-line* interaction: $t_i^{\min} \in [-L/2, L/2]$ and $t_j^{\min} \in [-L/2, L/2]$ (one case).
2. *Line-point* interaction between the segment i and an end-point of j: $t_i^{\min} \in [-L/2, L/2]$ and $t_j = \pm L/2$ (2 cases).
3. *Point-line* interaction between the segment j and an end-point of i: $t_j^{\min} \in [-L/2, L/2]$ and $t_i = \pm L/2$ (2 cases).
4. *Point-point* interaction between the end points of i and j: $t_i = \pm L/2$ and $t_j = \pm L/2$ (4 cases).

Our algorithm determines the Voronoi boundary between two rods as follows:

1. The configuration of the two rods is specified by the directions $\hat{t}_i$, $\hat{t}_j$, and the separation $\vec{r}$.
2. Choose a direction $\hat{s}$ in which the Voronoi boundary is to be determined at $\vec{s} = s\hat{s}$. The value of the boundary s will be a function of the configuration of the rods and $\hat{s}$:

$$s = s(\hat{t}_i, \hat{t}_j, \hat{s}, \vec{r}). \tag{6}$$

3. Solve Eq. (5) for each of the nine interaction cases. If the resulting s is real and positive it is a valid solution for the Voronoi boundary in the direction $\hat{s}$.

It is important to note that depending on the separation $\vec{r}$ and orientation of the two rods it is possible that two, or more, different types of interaction contribute to the Voronoi boundary for a given direction $\hat{s}$. This is illustrated in Fig. 2, where in the direction $\hat{s}'$ both line-line interactions and point-point interactions contribute. This ambiguity is considered in the algorithm, because for multiple contributing interactions one simply obtains multiple valid solutions for s.

IV. SOLUTION FOR THE DIFFERENT INTERACTIONS

We start by choosing a given direction $\hat{s}$ along which we will calculate the Voronoi boundary specified by s. The relevant scalar products between the unit vectors, $\hat{s}$, $\hat{r}$, $\hat{t}_i$ and $\hat{t}_j$ can be obtained. We consider the first interaction between the rods.

A. Line-line interaction

This case arises if the two solutions (3) fall inside the length of the segments. The conditions are:

$$t_i^{\min} \in [-L/2, L/2], \tag{7a}$$
$$t_j^{\min} \in [-L/2, L/2]. \tag{7b}$$

In this case t_i^{min} and t_j^{min} are given by Eqs. (3). Substituting these expressions into Eq. (5) then leads to a quadratic equation for the value s of the boundary:

$$\frac{s^2}{r^2}\Big[(\hat{st}_i)^2 - (\hat{st}_j)^2\Big] + 2\frac{s}{r}\Big[(\hat{st}_j)(\hat{rt}_j) - \hat{rs}\Big] + 1 - (\hat{rt}_j)^2 = 0. \tag{8}$$

Setting $l \equiv s/r$, the Voronoi boundary between the two rods thus scales with the separation r in this case:

$$s = r\, l(\hat{t}_i, \hat{t}_j, \hat{r}, \hat{s}), \tag{9}$$

where l is obtained from Eq. (8) and only depends on the four different directions.

B. Line-point interaction

In this case the solution for $t_i^{\min}$ falls along the line segment i and $t_j^{\min}$ is at one of the end points of rod j. We choose the top of $\vec{t}_j$ as the point (the other case is analogous) and we obtain:

$$t_i^{\min} = s(\hat{st}_i) \in [-L/2, L/2], \tag{10a}$$
$$t_j^{\min} = \frac{L}{2}, \tag{10b}$$

the second equation arises since

$$s(\hat{st}_j) - r(\hat{rt}_j) \notin [-L/2, L/2]. \tag{11}$$

Substituting the expressions Eq. (10) into Eq. (5) then leads to a quadratic equation for s:

$$\frac{s^2}{r^2}(\hat{st}_i) - \frac{s}{r}\Big[2(\hat{rs}) + \frac{L}{r}(\hat{st}_j)\Big] + \left(\frac{L}{2r}\right)^2 + \frac{L}{r}(\hat{rt}_j) + 1 = 0. \tag{12}$$

C. Point-line interaction

This interaction is analogous to line-point. We show the case when the point is at the top of $\vec{t}_i$. The conditions are:

$$t_i^{\min} = \frac{L}{2}, \tag{13a}$$
$$t_j^{\min} = s(\hat{st}_j) - r(\hat{rt}_j) \in [-L/2, L/2]. \tag{13b}$$

The first equation arises since

$$s(\hat{st}_i) \notin [-L/2, L/2]. \tag{14}$$

The quadratic equation resulting from Eq. (5) is then:

$$\frac{s^2}{r^2}(\hat{st}_j)^2 + 2\frac{s}{r}\Big[(\hat{rs}) - (\hat{st}_j)(\hat{rt}_j)\Big] - \\ -\frac{s}{r}\frac{L}{r}(\hat{st}_i) + \left(\frac{L}{2r}\right)^2 + \Big[(\hat{rt}_j)^2 \ -1\Big] = 0. \tag{15}$$

D. Point-point interaction

In this case the conditions are:

$$s(\hat{st}_i) \notin [-L/2, L/2], \tag{16a}$$
$$s(\hat{st}_j) - r(\hat{rt}_j) \notin [-L/2, L/2], \tag{16b}$$

so that the two points $t_i^{\min}$ and $t_j^{\min}$ are both fixed and equal to $L/2$ or $-L/2$.

We choose the values

$$t_i^{\min} = L/2, \tag{17a}$$
$$t_j^{\min} = L/2. \tag{17b}$$

Solving Eq. (5) with (17), we find:

$$s = r\,\frac{1 + \frac{L}{r}(\hat{rt}_j)}{2(\hat{rs}) + \frac{L}{r}((\hat{st}_j) - (\hat{st}_i))}. \tag{18}$$

The two line-point interactions and the point-point interaction do not scale with r except in the limit $L/r \to 0$, in this case from the point-point solution Eq. (18) we recover the Voronoi boundary between two hard spheres as calculated in [6, 7]:

$$s = \frac{r}{2(\hat{rs})}. \tag{19}$$

V. EXAMPLES OF SOLUTIONS AND DISCUSSION

As an example of the algorithm, we apply it to different situations in 2 dimensions, Fig. 3. We consider the rod i on the left and the rod j on the right. The top-left panel shows the Voronoi boundary in different colors corresponding to different interactions: a point-point interaction at the top of the boundary in red, then a point-line interaction in green, then a line-line interaction in blue, then another point-line interaction in green and so on. The other panels are analogous.

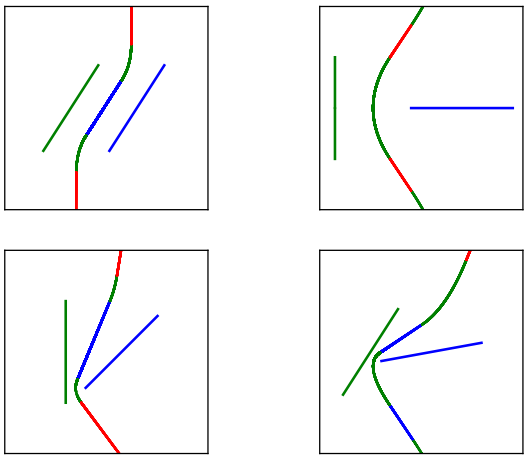

FIG. 3: Voronoi boundary in 2d for different situations. Each color of the boundary represents a type of interaction. Red = point-point, green = point-line and blue = line-line.

An important fact we should underline is that the three types of interactions are each composed by four (for point-point and point-line) or one (for line-line) of the nine surfaces. In dimension greater than 2 and for general angular configurations, the equation describing the surfaces of the point-line interaction and the line-line interaction are quadratic and the ones of the point-point interaction are linear. We thus obtain a surface made by a selection of four planes (due to the point-point interaction), four paraboloids of revolution (point-line) and one hyperbolic paraboloid (line-line) cut and paste together. In the limit $L \to \infty$, we only keep the hyperbolic paraboloid. The two dimensional case is special because the line-line equation always gives birth to a line. We thus obtain a curve made by a selection of five lines and four parabola.

The contribution of the different interactions, noted: C_{ll} for line-line, C_{pl} for point-line and C_{pp} for point-point, naturally changes with the ratio L/D and may lead to different trends in the behaviour of the volume fraction of the packing as a function of the aspect ratio, thus explaining the results of [14]. It is evident that for long but finite rods, C_{ll} will intervene much more than point interactions. Thus,

$$C_{pp} < C_{lp} < C_{ll}, \tag{20}$$

and reverse for small rods. We expect that:

(i) For very large ratio only C_{ll} needs to be considered.

(ii) For large ratio, only C_{ll} and C_{pl}.

(iii) For small ratio, only C_{pp} and C_{pl}.

(iv) For very small ratio (slightly deformed spheres), only C_{pp}.

These remarks are important to understand the behaviour of the volume fraction as a function of aspect ratio and will be analyzed in future works.

VI. CONCLUSION

We have shown how to calculate the Voronoi boundary between two spherocylinders as a boundary composed by analytical surfaces. The calculation of the Voronoi diagram for a set of spherocylinders is then possible as well as the calculation of the Voronoi volume. The analytical expression for the Voronoi boundary is highly simplified in the limit $L \to \infty$, i.e., in the Onsager limit for finite radius a, since only the solution scaling with r given by the line-line interaction Eq. (8) needs to be considered; the surface is then a hyperbolic paraboloid. The different solutions involving point interactions appear because of the finite extension of the spherocylinders and make the boundary more complicated and not scaling with r. These cases do not appear for infinite extension of the rods, thus Onsager limit corresponds to the simplest one.

The next step is to incorporate these expressions in order to calculate the excluded volume and excluded surface for two interacting particles. The statistical theory for the mean Voronoi volume of a rod should be similar to that of (multi disperse) spheres [10]. Thus, the calculation of the probability distribution to find a particle contributing to the Voronoi boundary can be performed. This calculation is analogous to the sphere case and can be performed by integrating over Theta functions as in [6–8]. In addition to the integration over the vector $\vec{r}$ one eventually also has to integrate over the possible directions of the rod j, $\hat{t}_j$. Such a calculation is in progress.

It is interesting to compare the case of rods of finite length to the one of infinite length. The thickness $D = 2a$ of the rods does not intervene in any of the formulas of the Voronoi boundary in both cases and will intervene only to determine the possible interactions. For spheres, we have approximated [9] the pair correlation function to a step function for the background term and a delta function for the contact term and, on average, this approximation has small influence on the final prediction of the volume fraction of the packing. For rods with infinite length, the pair correlation function (as a function of distance and angles) is equiprobable for non overlapping configurations as shown in [3]. This means that the approximation of [6, 9] for the background and contact

terms may becomes exact for infinite rods. For rods of finite length, the correlation function is not equiprobable, and considering the pair correlation function as a step-function becomes an approximation.

[1] G. J. Vroege and H. N. W. Lekkerkerker, Rep. Prog. Phys. **55**, 1241 (1992).
[2] P.-G. de Gennes. The physics of liquid crystals (Oxford, Clarendon, 1974).
[3] L. Onsager, Ann. N. Y. Acad. Sci. **51**, 627 (1949).
[4] S. F. Edwards and R. B. S. Oakeshott, Physica A **157**, 1080 (1989).
[5] S. Meyer, C. Song, Y. Jin, K. Wang and H. A. Makse, Physica A **389**, 5137 (2010).
[6] C. Song, P. Wang and H. A. Makse, Nature **453**, 629 (2008).
[7] C. Song, P. Wang, Y. Jin, H. A. Makse, Physica A **389**, 4497 (2010).
[8] P. Wang, C. Song, Y. Jin, H. A. Makse, Physica A **390**, 427 (2010).
[9] Y. Jin, P. Charbonneau, S. Meyer, C. Song and F. Zamponi, Phys. Rev. E **82**, 051126 (2010).
[10] M. Danisch, Y. Jin and H. A. Makse, Phys. Rev. E **81**, 051303 (2010).
[11] W. W. Wood and J. D. Jacobson, J. Chem. Phys. **27**, 1207 (1957).
[12] B. J. Alder and T. A. Wainwright, J. Chem. Phys. **27**, 1208 (1957).
[13] A. P. Philipse, Langmuir **12**, 1127 (1996).
[14] A. Donev, I. Cisse, D. Sachs, E. A. Variano, F. H. Stillinger, R. Connelly, S. Torquato, P. M. Chaikin, Science **303**, 990 (2004).
[15] Y. Jin and H. A. Makse, Physica A **389**, 5362 (2010).
[16] C. Radin, J. Stat. Phys. **131**, 567 (2008).
[17] D. Aristoff and C. Radin, J. Math. Phys. **51**, 113302 (2010).
[18] C. C. Mounfield and S. F. Edwards, Physica A **210**, 279 (1994).
[19] J. Blouwolff and S. Fraden, Europhys. Lett. **76**, 1095 (2006).

Acknowledgements. This work is supported by the National Science Foundation and Department of Energy. The authors would like to thank Jean-Marc Mercier and Yuliang Jin for helpful discussions.